

## Tomographic Reconstructions in RFX-mod via neural networks

L. Orlandi<sup>1,2</sup>, P. Franz<sup>1</sup>, V. Mutinelli<sup>3</sup>, G. Spizzo<sup>1,4</sup>, A. Rigoni Garola<sup>1</sup>, L. Piron<sup>1,5</sup>, E. Bucalo<sup>5</sup>

<sup>1</sup> *Consorzio RFX (CNR, ENEA, INFN, Università di Padova, Acciaierie Venete SpA),  
Corso Stati Uniti 4, 35127 Padova, Italy*

<sup>2</sup> *Centro Ricerche Fusione, Università di Padova, Padova, Italy*

<sup>3</sup> *ENI SpA, Piazza Ezio Vanoni, 1 - 20097 San Donato Milanese (MI)*

<sup>4</sup> *Istituto per la Scienza e la Tecnologia dei Plasmi (ISTP), CNR, Padova, Italy*

<sup>5</sup> *Dipartimento di Fisica e Astronomia, Università di Padova, Padova, Italy*

**Introduction** This work was conducted at Consorzio RFX in Padua, Italy, home to the world's largest reversed field pinch device, RFX-mod [1]. RFX-mod has achieved plasma currents up to 2 MA [2]. The machine is currently being upgraded to its next iteration, RFX-mod2 [3]. One of the challenges of RFP plasma diagnostics lies in the complex magnetic topologies that can emerge. In RFX-mod plasmas, Multiple Helicity (MH) and Single Helicity (SH) states can be observed. The MH regime is characterized by chaotic magnetic field lines, whereas the SH regime exhibits ordered, laminar magnetic structures [4-7]. Since soft x-ray (SXR) emissivity is closely linked to magnetic topology, SXR diagnostics are essential for understanding plasma dynamics and for advancing control and interpretation of plasma behavior. The goal of this study is to develop fast, accurate, and efficient tomographic inversion techniques for the SXR emission, reducing computational overhead without compromising reconstruction quality. A selected dataset of approximately 300 discharges, yielding around 70,000 pairs of line integrated brightness profiles and corresponding poloidal emissivity maps, forms the basis of this analysis. Two neural network models are evaluated: a Multi-Layer Perceptron (MLP) [8] that predicts the Fourier-Bessel coefficients of the emissivity map, and a transposed Convolutional Neural Network (tCNN) [9] that reconstructs the map directly from brightness data.

**Tomography Diagnostic** Soft X-ray tomography is a critical tool in magnetic confinement fusion research, offering high temporal resolution ( $\sim 10$  kHz in RFX-mod [11]) for tracking rapid emissivity fluctuations. It enables the reconstruction of 2D maps that reveal the time and spatial evolution of the plasma emissivity. Despite its utility, traditional tomographic reconstruction is computationally intensive, limiting its use to post-processing. The application of neural networks offers a path toward real-time emissivity mapping. With hardware acceleration (e.g., FPGA deployment [10]), trained models could deliver reconstructions during plasma experiments, significantly enhancing diagnostic capability. This study aims to identify

the most effective neural network approach for real-time SXR tomographic inversion in RFX-mod.

**Neural Networks Applications** Two distinct deep learning strategies for reconstructing SXR emissivity have been evaluated, the schematics of which are reported in Figure 1.:

**Multi-Layer Perceptron (MLP)** The MLP is a fully connected neural network that maps line-integrated brightness data directly to the Fourier-Bessel expansion coefficients of the emissivity field [11]. Given these coefficients and the known geometry of the diagnostic system, the 2D emissivity map is computed analytically through matrix multiplication. This architecture benefits from its simplicity and efficient training process, especially on limited datasets.

**Transposed Convolutional Neural Network (tCNN)** The tCNN approach bypasses the explicit geometric modeling by learning to reconstruct emissivity maps directly from brightness data. The network architecture is inspired by U-Net [12] and consists of dense input layers that expand the feature space, followed by multiple transposed convolutional blocks. These blocks iteratively upsample and refine the image representation, enabling the network to learn spatial features relevant to plasma geometry. Unlike the MLP, the tCNN does not require a priori knowledge of the diagnostic configuration, this is implicitly learned during training. However, this also makes the tCNN more data- and compute-intensive.

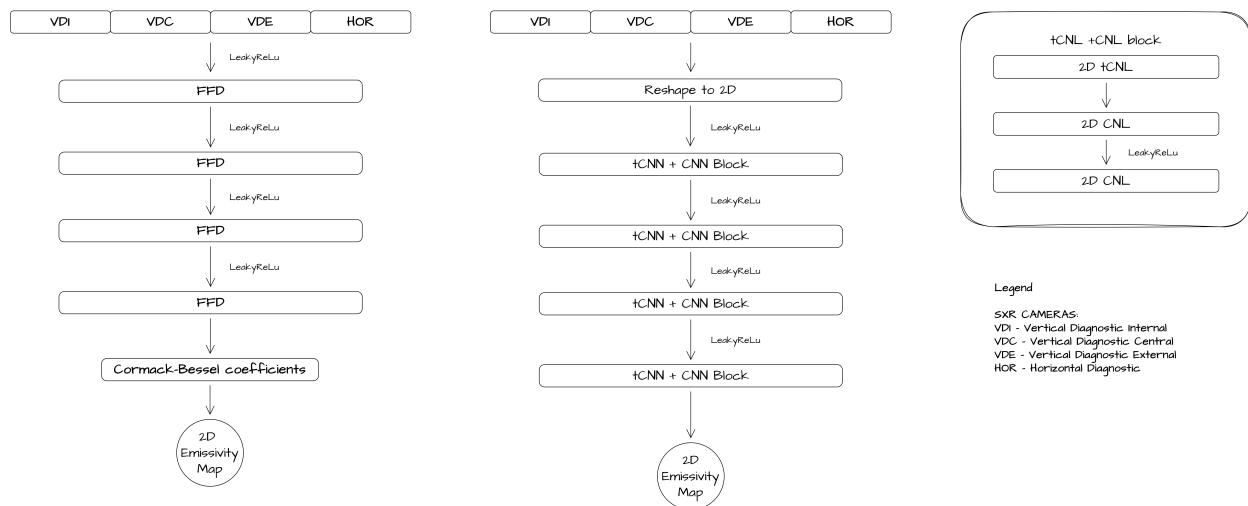


**Figure 1:** On the left is the MLP (Multilayer Perceptron) network, composed of four Fully Connected Forward (FFD) layers, where each neuron is connected to every neuron in the next layer. This is the most simple structure for a neural network. In the center and on the right is the architecture of the tCNN (transposed Convolutional Neural Network). Here, the input is first reshaped into a 2D matrix to enable the use of 2D convolutional operations. The network consists of four main blocks, the detail of which is given on the rightmost schema, each comprising one transposed convolutional layer, which increases the spatial resolution, followed by two standard convolutional layers to control the output dimensions. Convolutional layers were chosen to exploit the geometric structure of the lines of sight, allowing the network to better capture the spatial relationships between different camera views.

Both networks were optimized using the *Optuna* framework [13], which applies Bayesian optimization (via Gaussian Processes) to fine-tune hyperparameters such as learning rate,

architecture depth, activation functions, and, in the tCNN case, convolutional channel widths.

**Results and Discussion** Both neural networks demonstrate strong performance in reconstructing tomographic SXR emissivity maps from RFX-mod data, an example of such reconstructions is shown in Figure 2.

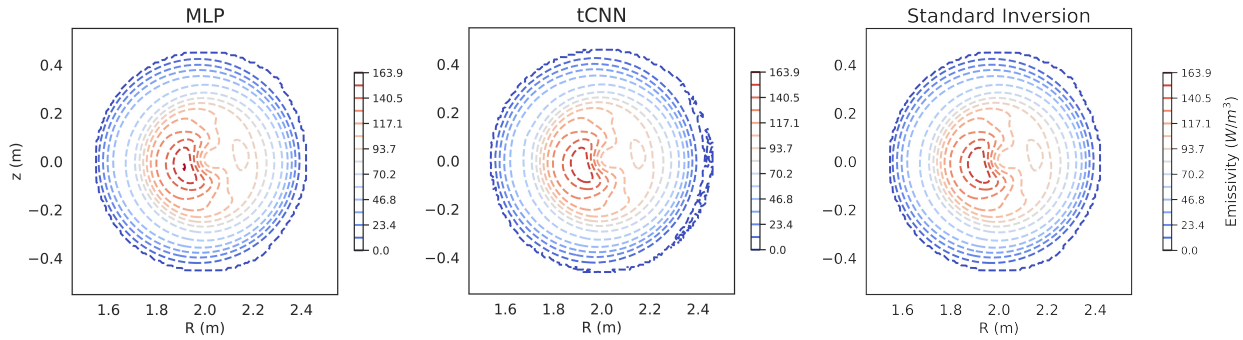


**Figure 2:** Examples of 2D emissivity map reconstructions. On the left the map obtained via the application of the MLP model, on the center the map corresponding to the tCNN model and on the right the ground truth map from the database

1. The MLP, leverages the multiple fully connected layers and the smaller 2D map representation given by the Fourier-Bessel coefficients, to achieve a mean absolute error (MAE) of  $\sim 0.46$  W/m<sup>3</sup> on the validation set. This corresponds to a relative error of  $\sim 0.5\%$ , given a mean emissivity of  $\sim 90$  W/m<sup>3</sup>.
2. The tCNN, while more complex, still performs well with an MAE of  $\sim 1.30$  W/m<sup>3</sup>, corresponding to a 1–2% relative error. The slightly higher error is likely due to the model's added burden of learning system geometry from data alone.

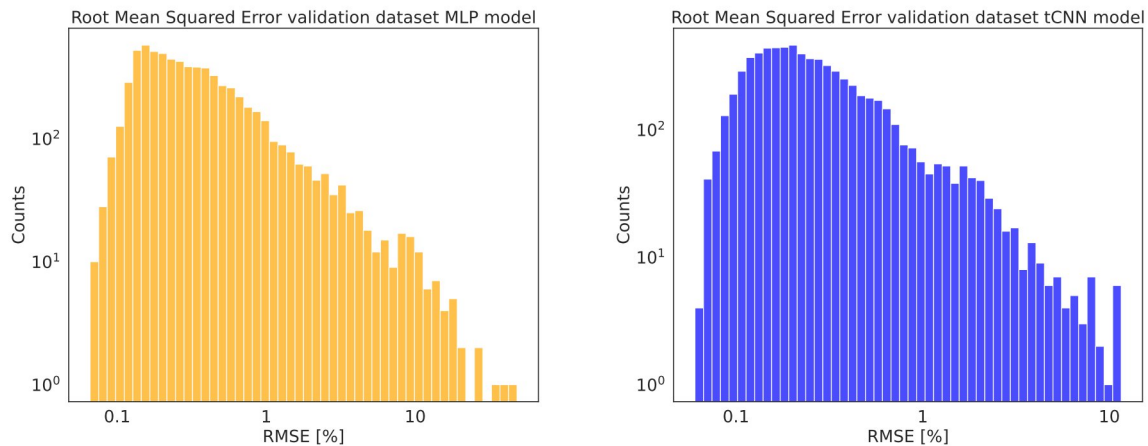


**Figure 3:** Root mean squared error (RMSE) distribution, for both models, computed over the validation dataset. On the left panel the error distribution for the MLP mode is shown, it is possible to see that it is peaked at around 0.3%. On the right panel the same quantity is displayed for the tCNN model, in this case the maximum of the distribution falls around 0.4%.

As mentioned above, it is possible to infer also from Figure 3 the error committed by the two models on the validation dataset. Despite the highlighted differences, both architectures produce reconstructions of sufficient quality for practical use. These results are particularly

encouraging given the moderate size of the training dataset, suggesting that even more accurate reconstructions could be achieved with larger databases or improved architectures. As far as the computational speed is concerned, both models offer a faster way to compute the inversion of the 2D emissivity maps. When compared against the validation dataset, that is comprised of 6935 couples of brightness-emissivity, the MLP managed to reconstruct all of the dataset with an average time of  $t_{\text{MLP}} = (4.3 \pm 0.1) \cdot 10^{-3}$  s, while the tCNN needs on average  $t_{\text{tCNN}} = (1.5 \pm 0.1) \cdot 10^{-3}$  s, this difference is due to the fact that while the tCNN has a more complex structure, it leverages the fewer connections between neurons in order to be faster. The promising performance of both models supports their potential for integration into real-time diagnostic systems, particularly in the upgraded RFX-mod2. With further development, such neural network-based tomographic tools could become standard instruments in fusion research, offering rapid, high-fidelity insights into plasma behavior.

**Conclusions** This study demonstrates the viability of neural networks for fast and accurate SXR tomographic inversion in RFX-mod plasmas. Both MLP and tCNN models deliver strong performance, with the MLP excelling in simplicity and precision, and the tCNN offering more architectural flexibility. These methods open the door to real-time emissivity reconstruction, a crucial capability for active plasma control and live diagnostics in next-generation fusion devices. Future work will involve scaling the training dataset, refining network architectures, and exploring deployment on low-latency hardware systems such as FPGAs.

## References

- [1] P. Sonato et al 2003 *Fus. Eng. Des.*, 66–68, pp. 161-168 [10.1016/S0920-3796\(03\)00177-7](https://doi.org/10.1016/S0920-3796(03)00177-7)
- [2] P. Martin et al 2011, *Nucl. Fusion* [10.1088/0029-5515/51/9/094023](https://doi.org/10.1088/0029-5515/51/9/094023)
- [3] S. Peruzzo et al 2019 *Fus. Eng. Des.* Vol. 146, pp. 692-696; [10.1016/j.fusengdes.2019.01.057](https://doi.org/10.1016/j.fusengdes.2019.01.057)
- [4] Lorenzini, R., Martines, E., Piovesan, P. et al. *Nature Phys* 5, 570–574 (2009). [10.1038/nphys1308](https://doi.org/10.1038/nphys1308)
- [5] P. Franz et al 2013 *Nucl. Fusion* **53** 053011 [10.1088/0029-5515/53/5/053011](https://doi.org/10.1088/0029-5515/53/5/053011)
- [6] Gobbin et al *Phys. Plasmas* 18, 062505 (2011) [10.1063/1.3602083](https://doi.org/10.1063/1.3602083)
- [7] P. Franz et al 2001 *Nucl. Fusion* 41 695 [10.1088/0029-5515/41/6/304](https://doi.org/10.1088/0029-5515/41/6/304)
- [8] Almeida, Luis B (2020) [1996]. "Multilayer perceptrons". [10.1201/9780429142772](https://doi.org/10.1201/9780429142772)
- [9] Dumoulin, V.; Visin, F. (2018). [10.48550/arXiv.1603.07285](https://arxiv.org/abs/1603.07285)
- [10] A. Rigoni Garola et al. *IEEE Transactions on Nuclear Science*, vol. 68, no. 8, pp. 2165-2172 [10.1109/TNS.2021.3096837](https://doi.org/10.1109/TNS.2021.3096837)
- [11] A. M. Cormack, *J. Appl. Phys.* 34, 2722 (1963). [10.1063/1.1729798](https://doi.org/10.1063/1.1729798)
- [12] O. Ronneberger et al. *MICCAI 2015*, Springer. [10.1007/978-3-319-24574-4\\_28](https://doi.org/10.1007/978-3-319-24574-4_28)
- [13] Takuya Akiba, Shotaro Sano, Toshihiko Yanase, Takeru Ohta, and Masanori Koyama. 2019. Optuna: A Next-generation Hyperparameter Optimization Framework. In *KDD.c*